A&A 433, 285–295 (2005)
DOI: 10.1051/0004-6361:20040507

Astronomy & Astrophysics

Abundance correlations in mildly metal-poor stars

II. Light elements (C to Ca)⋆

H. Decauwer[1], E. Jehin[2], G. Parmentier[3], and P. Magain[1]

[1] Institute of Astrophysics and Geophysics, University of Liège, 17 Allée du 6 Août, 4000 Liège, Belgium
e-mail: decauwer@astro.ulg.ac.be
[2] European Southern Observatory, Casilla 19001, Alonso de Cordova 3107, Vitacura, Santiago, Chile
[3] Institute of Astronomy, University of Cambridge, Madingley Road, Cambridge CB3 0HA, UK

Received 23 March 2004 / Accepted 16 November 2004

Abstract. Accurate relative abundances have been obtained for carbon, oxygen, sodium, aluminium, silicon, and calcium in a sample of mildly metal-poor stars. This analysis complements a previous study carried out by Jehin et al. (1999, A&A, 341, 241), which provided the basis for the EASE scenario. This scenario postulates that field metal-poor stars were born in self-enriched proto-globular cluster clouds. By further investigating the correlations between the different α-element abundances, we propose a modified scenario for the formation of intermediate metallicity stars, in which the stars exhibiting lower than average α/Fe abundance ratios would form in low mass clouds, unable to sustain the formation of very massive stars ($M \gtrsim 30\ M_{\odot}$). Moreover, the carbon-to-iron ratio is found to decrease as one climbs the so-called Population IIb branch, i.e. when the *s*-element abundance increases. In the framework of the EASE scenario, we interpret this anticorrelation between the carbon and the *s*-element abundances as a signature of a *hot bottom burning* process in the metal-poor AGB stars which expelled the matter subsequently accreted by our Population IIb stars.

Key words. stars: abundances – stars: Population II – stars: atmospheres – nuclear reactions, nucleosynthesis, abundances – Galaxy: evolution

1. Introduction

In a previous study (Jehin et al. 1999), we had obtained accurate relative abundances for a sample of 21 mildly metal-poor stars ([Fe/H] ~ -1), whose metallicities are characteristic of the disk-halo transition. The main emphasis was on the study of the neutron-capture elements, both from the *s*- and the *r*-processes.

The high precision of the derived abundances allowed us to investigate in great detail the correlations between the relative abundances of the elements considered. The most spectacular result was the discovery of a quite peculiar relation between the *s*-process element and the α-element abundances, forming what we called the "two-branches diagram" (Fig. 1).

This behaviour led us to conclude that the metal-poor (i.e., Population II) stars could be separated into two subpopulations: Pop IIa, with a variable [α/Fe] and a constant or slowly varying [*s*/Fe], and Pop IIb, with a maximum [α/Fe] and various values of [*s*/Fe], but higher than for Pop IIa. In the correlation diagram between the [Y/Fe] and [Ti/Fe] abundance ratios (Fig. 1), Pop IIa and Pop IIb correspond to the low and vertical branches of the "two-branches diagram", respectively. (To remain consistent with Jehin et al. (1999), we keep the labels Pop IIa and Pop IIb although we acknowledge that

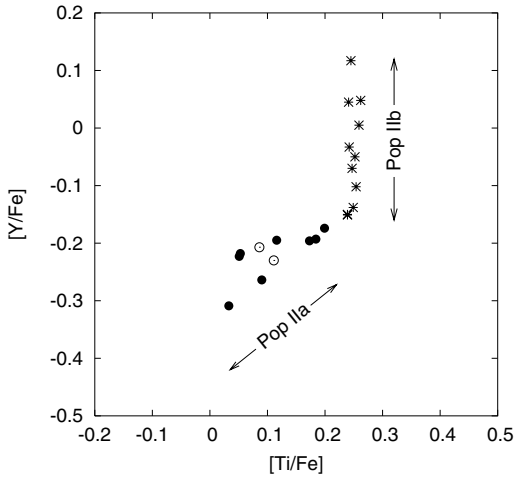

Fig. 1. Two-branches diagram. Filled circles and asterisks represent population IIa and IIb stars, respectively. Open circles represent two peculiar population IIa stars (see text for details).

⋆ Based on observations collected at the European Southern Observatory, La Silla, Chile (ESO Programmes 56.E-0384, 57.E-0400 and 59.E-0257).

many stars in the metallicity range considered do not belong to Population II.)

In order to explain this peculiar behaviour, we proposed a scenario in which the field metal-poor stars were all born in proto-globular cluster clouds (hereafter PGCCs) made of primordial gas, during an early phase of the Galactic evolution.

According to this scenario, the proto-galaxy, which is made of primordial gas, fragments into a number of gas clouds, the PGCCs, of various masses. In the center of these primordial clouds, a first generation of zero metallicity stars forms. Owing to the absence of metals, these first generation stars possibly form with an initial mass function (IMF) biased towards massive stars (e.g. Larson 1998; Nakamura & Umemura 1999). These massive stars rapidly evolve and end their lives exploding as type II supernovae (SNeII).

These SNII explosions induce a shock wave in the PGCC, turning it into an expanding supershell. This dense shell of gas may encounter physical conditions favourable to its transverse collapse and, thus, to the triggered formation of a second stellar generation (Parmentier 2004). This triggered formation is more efficient than the formation of first generation stars and a much larger fraction of the PGCC gas is now turned into stars. These second generation stars also form with a higher metallicity due to the mix of SN processed material with pristine gas, and, thus, have a more classical IMF. The metallicity achieved at the end of the self-enrichment process depends on the PGCC mass (i.e., the mass of primordial gas to be chemically enriched) as well as on the amount of metals ejected by the massive stars of the first generation into the interstellar medium.

At this stage, the shell of newly formed stars, which forms the proto-globular cluster (PGC), may recondense under its own gravitation (and thus form a star cluster), or may be disrupted if its gravitational energy is lower than the kinetic energy of the supershell (Brown et al. 1995). In the latter case, the second generation stars are scattered in the Galactic halo and become field Pop IIa stars.

If the PGC is sufficiently bound, a globular cluster (GC) forms, mostly constituted of second generation stars, with possibly a tiny fraction of first generation low mass stars (Parmentier et al. 1999). The remaining interstellar gas, which is much less dense than in the PGCC, is unable to retain the matter expelled at high velocities by SNeII of the second generation (as well as type I SNe of any generation). Thus, SNe do not contribute anymore to the chemical evolution of the GC.

However, some processed material is also expelled, at much lower velocities, by intermediate mass stars on the asymptotic giant branch (AGB). Provided that the gravitational potential of the GC is high enough, that matter will remain bound to the cluster and will form a reservoir of gas in the GC central regions. Cluster stars will accrete part of this gas while crossing the reservoir. They will thus display a surface composition which is modified by the AGB-processed material and, in particular, they will display overabundances in *s*-process elements. If some of these stars later escape the cluster (either by gradual evaporation or because of total cluster disruption) and become field stars, they will form Pop IIb. Their location along the second branch of the [Y/Fe] versus [α/Fe] diagram will be related to the efficiency of the accretion process which has previously taken place in the GC where the stars were born, that is, the more efficient the accretion process, the larger the [Y/Fe] ratio.

This EASE scenario (standing for Evaporation/ Accretion/Self-Enrichment), which was devised to interpret the observed abundance correlations, subsequently proved to be able to explain the observed metallicities of present-day Galactic halo GCs (Parmentier et al. 1999) as well as the distance-metallicity relation for the subgroup of Galactic GCs belonging to the Old Halo (Parmentier et al. 2000) and the mass-metallicity relation found for the same subgroup (Parmentier & Gilmore 2001).

This scenario was built on the observations of α-element and neutron-capture element abundances. But no result was obtained for the lighter elements, among which carbon plays a key role, both in SN and in AGB nucleosynthesis. The purpose of the present paper is to complement the Jehin et al. (1999) results with abundances of carbon, oxygen, sodium and aluminium.

Table 1. Line data. The columns give, respectively, the element and its ionization stage or the molecule used, the wavelength, the excitation potential of the lower level, the $\log gf$ taken from the literature and the equivalent width in the spectrum of HD 203608. Note that the results concerning the first two lines of Ca come directly from Jehin et al. (1999).

Line	λ (Å)	χ (eV)	$\log gf$	EW (mÅ)
CH	4313.610	0.021	−1.379	38.6
CH	4328.610	1.315	−0.690	11.9
CH	4329.340	1.257	−0.694	20.0
[O I]	6300.311	0.000	−9.750	1.7
O I	7771.954	9.150	0.369	72.2
O I	7774.177	9.150	0.223	62.2
O I	7775.395	9.150	0.002	47.2
Na I	5682.647	2.100	−0.700	45.2
Na I	6154.230	2.100	−1.543	9.2
Na I	6160.753	2.100	−1.275	18.2
Al I	7835.317	4.020	−0.800	9.3
Al I	7836.130	4.020	−0.630	11.8
Si I	5690.433	4.930	−1.766	16.9
Si I	5701.108	4.930	−1.947	12.0
Si I	6125.026	5.610	−1.534	10.1
Si I	6142.494	5.620	−1.425	10.6
Si I	7800.000	6.180	−0.669	21.5
Ca I	4108.532	2.710	−0.829	24.0
Ca I	4578.559	2.520	−0.697	42.9
Ca I	6161.295	2.520	−1.194	22.5
Ca I	6166.440	2.520	−1.081	26.5

2. Observational material and abundance analysis

The carbon abundances were determined from the analysis of CH lines present in the spectra of Jehin et al. (1999). We selected three clean features in the CH *G*-band, one of which is a single line, and the other two are close blends of two CH lines of the same excitation potential. These features are listed in Table 1 and a sample spectrum is shown in Fig. 2.

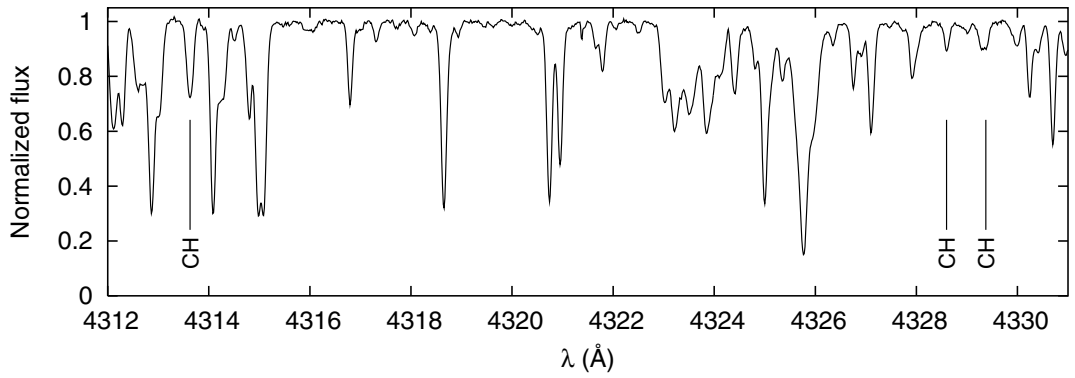

Fig. 2. Part of HD 76932 spectrum around the CH lines analyzed.

As no oxygen lines were present in the original Jehin et al. (1999) data, additional spectra were obtained with the same telescope and spectrograph (ESO CAT + CES at La Silla), but with the Very Long Camera. Two regions were observed, the first priority being the region around the forbidden line of O I at 6300 Å, the second priority the infrared triplet around 7770 Å. The ranges of observed wavelengths were approximately [6280, 6350] and [7760, 7840] Å and the resolution was about 60 000. These spectra were reduced in the standard way (bias and sky subtraction, flat fielding, optimal extraction, wavelength calibration). The continuum level was determined on the basis of continuum windows preselected from inspection of the Liège solar atlas (Delbouille et al. 1973). As we had only one observing run, not all 21 stars were observable during that period. We obtained spectra of the forbidden line for 13 stars. In five of them, the line was either not detected or blended with the telluric emission. We are thus left with a subsample of 8 stars, to which we could add 3 stars in which the forbidden oxygen line was measured by Nissen et al. (2002) on spectra of similar precision to ours.

The infrared triplet forms in deep layers; it is thus very sensitive to temperature. Moreover, it is well known to be affected by departures from LTE (see, e.g., Cavallo et al. 1997). In eight stars for which we have both the forbidden line and the infrared triplet, we find that the latter gives an abundance ~0.4 dex higher than the more reliable forbidden line, with a scatter of 0.1 dex. Note that, for the 6300 Å line, we have taken into account a slight blending by a Ni I line (Nissen et al. 2002), although it was almost negligible (from 0.1 to 0.2 mÅ). For that, we have calculated the value of the Ni I line equivalent width using the Ni abundance deduced from other lines in Jehin et al. (1999).

In order to check the precision of our two oxygen abundance indicators, we have compared [O/Fe] with [Mg/Fe], magnesium being an α-element like oxygen, and the closest in the periodic table which can be measured. Most of O and Mg are expected to be synthesized by the same nucleosynthetic processes in massive stars and we thus expect their abundances to vary in concert. The [O/Fe] versus [Mg/Fe] diagram is presented in Fig. 3, with the O abundance as determined from the forbidden line (left panel) and from the infrared triplet (right panel). It is clear that the correlation is much better when the forbidden oxygen line is used. Strictly speaking, this is not a proof that the forbidden line constitutes a better abundance indicator than the infrared triplet. However, this is a strong argument pointing in that direction, and confirming the expectations. We thus decided to disregard the O abundances obtained from the infrared triplet and to use the forbidden line as our sole abundance indicator for oxygen.

Along with the two regions observed for the oxygen lines, a third spectral region was observed with the same instrument in the wavelength range [6110, 6180] Å. It allowed us to analyze two Na I lines, two Si I lines and two Ca I lines. The two Ca I lines used by Jehin et al. (1999) were added to ours so that a more precise Ca abundance was derived. For Na and Si, we also used equivalent widths (EW) deduced by Magain (private communication) in another program with the CES and the Long Camera for 12 stars of the sample. The aluminium abundance has been determined from two lines of Al I present in the same spectra as the oxygen infrared triplet.

All the line data we used are listed in Table 1. The obtained abundances are listed in Table 2.

The abundances were determined using the same model atmospheres as Jehin et al. (1999), so that our results are directly comparable to theirs. Note that Jehin et al. determined abundance ratios, whenever possible, from indicators having very similar sensitivities to the atmospheric parameters, in order to minimize errors due to uncertainties in these parameters (effective temperature, surface gravity, metallicity, microturbulence velocity). We also tried to adopt the same philosophy. Unfortunately, this is not possible when comparing carbon to any other element, the CH lines having quite different sensitivities to temperature and pressure in comparison with our metallic lines.

As we are interested in comparing abundance ratios in the different stars of our sample, and not so much in the absolute abundances, the crucial point is the internal precision of our results and, consequently, the internal precision of our atmospheric parameters. Indeed, a zero point shift of, e.g., all our effective temperatures would basically shift the abundance ratios in all stars by the same amount, and would not affect our star-to-star comparisons.

Thus, the errors in the abundance ratios are determined from the internal uncertainties in the atmospheric parameters. For $T_{\rm eff}$, Jehin et al. used two colour indices $(b-y)$ and $(V-K)$ and concluded, on the basis of the comparison between these

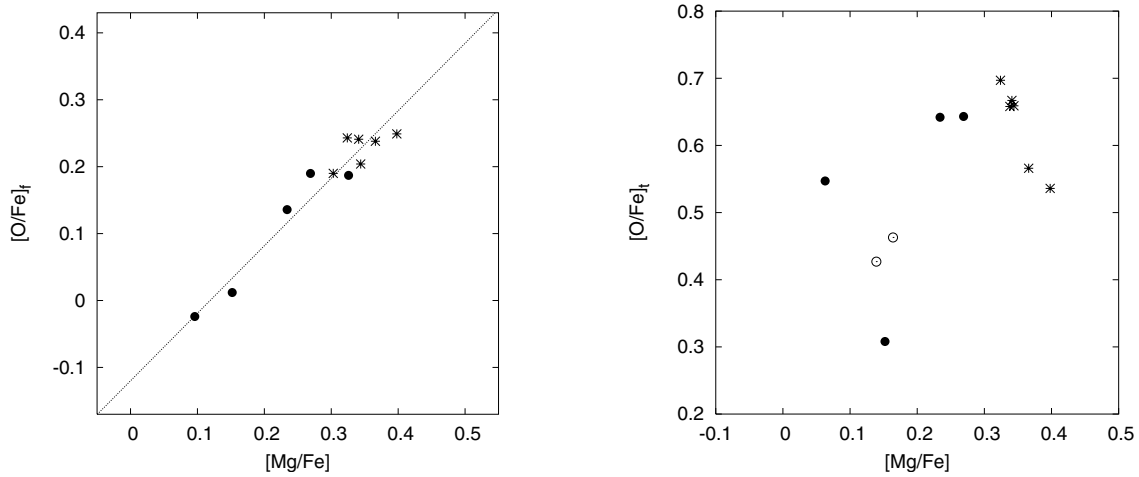

Fig. 3. Correlation diagrams for [O/Fe] versus [Mg/Fe] for the stars from which abundances have been deduced from the forbidden line (*left panel*) and from the triplet (*right panel*). Symbols are the same as in Fig. 1.

Table 2. Obtained abundances. The different parts of the table correspond to Pop IIa, Pop IIb and peculiar stars, respectively.

HD	[Fe/H]	[C/Fe]	[O/Fe]	[Na/Fe]	[Al/Fe]	[Si/Fe]	[Ca/Fe]
25 704	−0.960	−0.347	+0.190	+0.066	+0.354	+0.170	+0.130
59 984	−0.755	−0.221	*	*	*	*	+0.055
61 902	−0.727	−0.138	*	+0.095	*	+0.082	+0.040
111 971	−0.737	−0.255	−0.024	−0.055	*	+0.172	+0.047
134 169	−0.804	−0.247	+0.187	+0.012	*	+0.181	+0.138
152 924	−0.708	−0.199	+0.136	+0.092	+0.142	+0.273	+0.129
203 608	−0.677	−0.175	+0.012	+0.095	+0.061	+0.093	+0.000
215 257	−0.804	−0.366	*	+0.105	+0.311	+0.169	+0.085
22 879	−0.892	−0.262	+0.204	+0.059	+0.137	+0.282	+0.200
63 077	−0.831	−0.287	*	*	*	*	+0.165
63 598	−0.856	−0.240	*	+0.048	*	+0.246	+0.175
76 932	−0.910	−0.264	+0.238	+0.048	*	+0.262	+0.232
78 747	−0.730	−0.252	*	*	*	*	+0.178
79 601	−0.668	−0.202	*	+0.099	*	+0.216	+0.188
97 320	−1.220	−0.090	+0.190	+0.046	*	+0.215	+0.159
126 793	−0.800	−0.197	+0.241	+0.100	+0.356	+0.299	+0.183
189 558	−1.129	−0.347	+0.249	−0.086	+0.327	+0.294	+0.231
196 892	−1.031	−0.217	+0.243	+0.012	+0.277	+0.311	+0.217
199 289	−1.074	−0.221	*	+0.062	+0.310	+0.262	+0.163
193 901	−1.071	−0.439	*	−0.308	−0.091	+0.025	+0.118
194 598	−1.126	−0.252	*	−0.143	−0.103	+0.098	+0.144

two indicators, that the internal precision was 20 K. The microturbulence velocity precision, estimated from the scatter in the *EW* versus abundance plots, amounts to 0.1 km s^{-1}.

For the surface gravity and the metallicity, Jehin et al. (1999) adopted rather arbitrarily uncertainties of 0.2 dex. This is far too pessimistic for the internal precision, and probably more representative of the external accuracy. Indeed, the internal precision of [Fe/H], taking into account *EW* errors, as well as errors in all atmospheric parameters, amounts to 0.02 dex only, which we adopt as our uncertainty in the metallicity.

Jehin et al. (1999) determined their surface gravities from the c_1 index of Strömgren photometry. We have estimated the uncertainty in this parameter by comparing these photometric values with spectroscopic ones, determined from the three ionization equilibria of Fe, Cr and Ti. The mean difference between the spectroscopic and photometric gravities amounts to 0.02 dex, with a scatter of 0.11 dex. This scatter is taken as our estimate of the internal precision of the photometric gravities (indeed, it should rather be considered as an upper limit, since both the uncertainties in spectroscopic and photometric gravities contribute to the scatter).

The uncertainties in the various abundance ratios caused by atmospheric parameters are summarized in Table 3.

3. Results and discussion

The abundances of carbon, oxygen, sodium and aluminium relative to iron are plotted against the metallicity index [Fe/H] in Figs. 4 and 5. The C/Fe ratio appears subsolar for all stars of

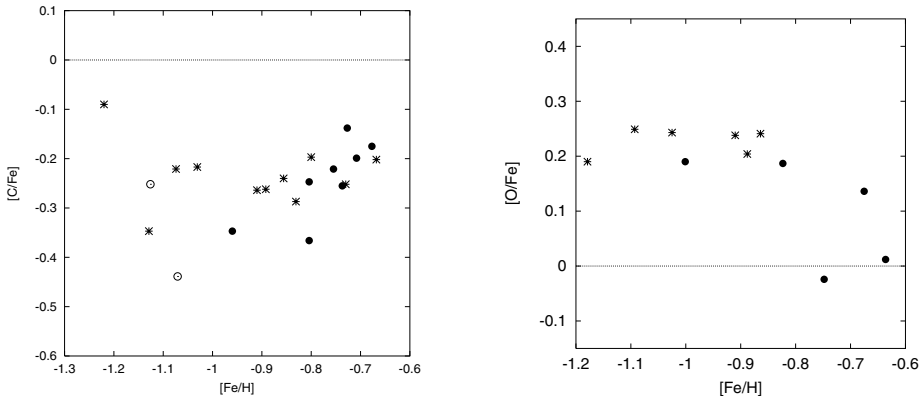

Fig. 4. Abundances of C and O relative to Fe versus [Fe/H]. Symbols are the same as in Fig. 1.

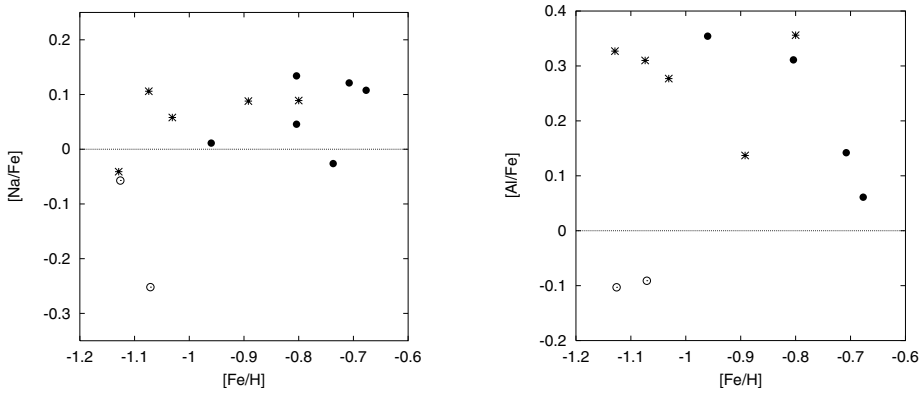

Fig. 5. Abundances of Na and Al relative to Fe versus [Fe/H]. Symbols are the same as in Fig. 1.

Table 3. Influence of errors in the model parameters on the HD 76932 abundances. The f and t indices beside the O/Fe ratios refer to the O abundance obtained from the forbidden line and from the triplet, respectively.

Element abundance	$\Delta T_{\rm eff}$ +20K	$\Delta \log g$ +0.11	Δ [Fe/H] +0.02	$\Delta\xi$ +0.1	rms sum
[C/Fe]	+0.014	−0.031	+0.008	+0.008	0.036
$[O/Fe]_{\rm f}$	+0.007	−0.008	+0.004	+0.008	0.014
$[O/Fe]_{\rm t}$	−0.020	−0.016	+0.000	−0.004	0.026
[Na/Fe]	−0.005	−0.006	+0.001	+0.008	0.011
[Al/Fe]	−0.008	−0.008	+0.000	+0.008	0.014
[Ca/Fe]	−0.004	−0.007	+0.001	+0.003	0.009
[Si/Fe]	−0.009	−0.001	+0.001	+0.008	0.012

our sample, and increases slightly towards the solar value as the metallicity becomes closer to solar. The most metal-poor star of the sample, HD 97320, seems to depart from this trend, being also the least depleted in carbon.

In agreement with the usual results (see for instance Cavallo et al. 1997), we find that oxygen is overabundant relative to iron in metal-poor stars, at least below [Fe/H] ~ -0.8, and decreases towards the solar value at higher metallicities. The Na/Fe ratio is close to solar, while Al appears slightly overabundant in most stars analyzed.

3.1. Anomalous stars

As was already pointed out by Jehin et al. (1999), two stars depart significantly from the general relations: HD 193901 and HD 194598. When compared to the other program stars, these two stars were found to display clear overabundances in r-process elements, while nickel and the α-elements are somewhat underabundant relative to iron. Our complementary study confirms their peculiarity, with Na and Al displaying significantly lower than average abundances.

Combining our results with those of Jehin et al., we can conclude that, when they are compared to other stars of similar metallicities, the chemical composition peculiarities of these two stars are as follows: while Cr behaves like Fe, the r-process elements appear overabundant, and Na, Al, V, Ni and all the α-elements are underabundant. In such a situation, where most of the elements analyzed are underabundant relative to Fe, it might appear more appropriate to describe the chemical composition peculiarities as a moderate overabundance of Fe and Cr combined with an even larger overabundance of r-process elements.

Kinematically, Jehin et al. noted that these two stars also differ from the rest of the sample. While the other 19 stars have rather low eccentricity orbits, i.e., typical of the thick disk or of the inner halo, these two anomalous stars show high eccentricities linking them to the outer halo. In order to further investigate the possible chemical composition peculiarities in outer

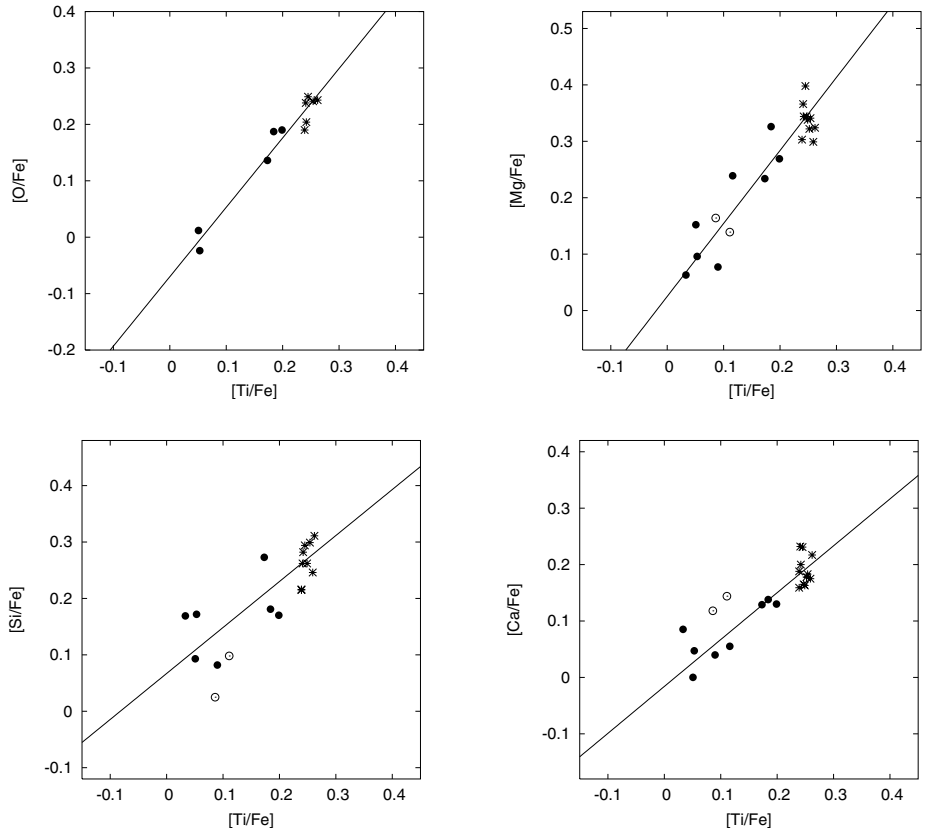

Fig. 6. Abundances of O, Mg, Si and Ca relative to Fe versus [Ti/Fe] (*top left*, *top right*, *bottom left* and *bottom right*, respectively). Symbols are the same as in Fig. 1. Solid lines represent the fits.

Table 4. Slopes of the regression lines for the α-elements.

Abundance ratios	Slope
[O/Fe] vs. [Ti/Fe]	1.21 ± 0.14
[Mg/Fe] vs. [Ti/Fe]	1.21 ± 0.10
[Si/Fe] vs. [Ti/Fe]	0.76 ± 0.06
[Ca/Fe] vs. [Ti/Fe]	0.81 ± 0.05

halo stars, we have now started a much more detailed study of a sample of outer halo stars.

3.2. Alpha elements

Considering our results together with those of Jehin et al. (1999), the abundances of five α-elements, namely O, Mg, Si, Ca and Ti are now available. The abundances of the first four relative to Fe are plotted versus [Ti/Fe] in Fig. 6, which shows that these abundances are nicely correlated. However, the slopes of the best fit lines in these diagrams differ significantly from unity. We have determined these slopes by a least squares fit, taking into account errors in both coordinates, estimated as described in Sect. 2, and excluding the two anomalous stars. The results are summarized in Table 4.

Figure 6 and Table 4 show that the two lightest α-elements considered in this study, O and Mg, have the same behaviour, with a slope > 1 when compared to Ti, i.e. a range of variation which is significantly larger than the one of Ti. On the contrary, the two heavier α-elements, Si and Ca, which also behave in the same way, present a slope < 1, and thus show less variation than Ti (and, of course, than O and Mg).

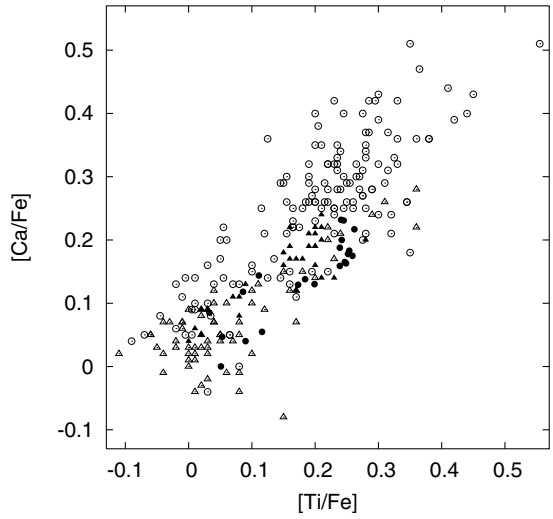

Fig. 7. [Ca/Fe] versus [Ti/Fe] from different analyses: present paper (solid circles), Nissen & Schuster (1997, solid triangles), Bensby et al. (2003, open triangles), and Gratton et al. (2003, open circles).

In order to check if these results are compatible with previous studies, we have considered the analyses of Nissen & Schuster (1997), Bensby et al. (2003, thin disk stars excluded) and Gratton et al. (2003). The results for [Ca/Fe] versus [Ti/Fe] are plotted together in Fig. 7. All analyses support the correlation with a slope lower than unity, ranging from 0.66

(Nissen & Schuster 1997) to 0.91 (Bensby et al. 2003). However, the scatter around the mean curve, which amounts to 0.029 dex in our study and is the same for Nissen & Schuster (1997), increases to 0.057 in Bensby et al. (2003) and 0.064 in the Gratton et al. (2003) data, which suggests that the latter two studies, which deal with more stars, are of somewhat lower precision (and this is even more true for other α-elements).

If one accepts the idea that these α-elements have been mostly synthesized in massive (i.e., $M > 8\ M_{\odot}$) stars, the different slopes exhibited by the light and heavy α-elements suggest that the yields of the lighter α-elements O and Mg vary more strongly with the star mass than those of the heavier ones Si and Ca. The abundance of Ti, the heaviest one, behaves in an intermediate way. It might be argued that at least part of the synthesis of Ti could be linked to the iron peak nucleosynthesis rather than to α-elements nucleosynthesis. However, the correlations found in the present study and in Jehin et al. (1999) show that, in the metallicity range considered here ([Fe/H] ~ -1), Ti behaves much more like an α-element than like an iron-peak element.

3.3. Problems with the original EASE scenario

According to the original EASE scenario, the stars of the Pop IIa branch were formed in a shell whose formation and expansion had been promoted by the explosions of the first generation SNeII. The variation of [α/Fe] was explained in the following way.

If the star formed at the very beginning of the SNeII phase, its gas would have been enriched by few SNeII and, thus, the [α/Fe] ratio would be low and the star would lie at the left edge of the branch. If the star formation took place at a later time, the gas would be more enriched in α-elements and the star would present a higher [α/Fe]. Finally, if the star formed at the end of the SNeII phase, [α/Fe] would be maximum, that is, the star would be located at the right edge of the first branch.

This version of the scenario is unable to explain the detailed behaviour of the α-elements abundances highlighted in Table 4 and Fig. 6. Indeed, recent nucleosynthesis models for SNeII (e.g., Umeda & Nomoto 2002) show that the largest amount of the lighter α-elements as compared to the heavier ones is produced by the most massive stars. E.g., the highest O/Si or Mg/Ca is produced by the most massive (and shortest lived) SNeII. Thus, the highest O/Si and Mg/Ca should be found in stars formed at the beginning of the SNeII phase and, thus, in the left part of the Pop IIa branch. Exactly the reverse is observed: O/Si and Mg/Ca are lowest at the left edge of the branch and grow towards the right edge.

In other words, the dependence of the SNII yields on the SNII progenitor mass implies that the second generation stars displaying the largest light/heavy elements ratio (e.g., O/Si, Mg/Ca) were formed at the *beginning of the SNII phase*, when the interstellar gas was polluted by the ejecta of the most massive stars only.

Regarding the abundance ratios measured with respect to iron, the models also show that the most massive stars produce the highest [α/Fe] ratios[1]. Again, this is exactly opposite to the original EASE scenario in which the stars at the right edge of the first branch, thus with the largest [α/Fe] ratio, are supposed to form at the end of the SNII phase. This problem had already been pointed out by Nissen (1999).

3.4. The standard scenario

If the original EASE scenario encounters problems in explaining the observed abundance ratios, one might be tempted to come back to a more classical model, which we shall call *the standard scenario*.

In the standard scenario, the primordial matter is first enriched by the ejecta of type II SNe (which, being the most massive stars, are expected to explode first). Thus, the oldest stellar populations display the high α/Fe ratios characteristic of SNeII ejecta. Afterwards, type Ia SNe start to explode and enrich the interstellar gas with matter containing a higher proportion of Fe-peak elements. Contrary to the original EASE scenario, the standard one thus predicts that the α/Fe ratio decreases with time. This scenario is generally invoked to explain the chemical evolution of the Galactic disk, and we think that it basically applies at metallicities typical of the thin disk ($-0.6 \lesssim$ [Fe/H] $\lesssim 0$). The question here is: does it also apply at the lower metallicities ([Fe/H] ~ -1) considered here?

First, if we can trust the still uncertain yields of type Ia SNe (e.g. Iwamoto et al. 1999), which predict that the heaviest α-elements are more efficiently produced than the lightest ones, this could explain the observed variations between the α-elements themselves. Indeed, if Si and Ca are more efficiently produced than O and Mg, the Si/Fe and Ca/Fe ratios should decrease more slowly with time than O/Fe and Mg/Fe.

However, in the framework of this standard scenario, since the SNIa ejecta enrich the interstellar gas, the decrease of α/Fe would go together with an increase of metallicity. Indeed, if one accepts that this process makes it possible to explain the chemical evolution of the Galactic disk, one notes that a decrease of $\sim$0.3 dex in α/Fe occurs together with an increase of metallicity from ~ -0.6 to 0. In order to test if this standard scenario can explain the behaviour observed at the lower metallicities considered in the present analysis, one should check that the decrease in α/Fe along the Pop IIa branch is accompanied by a similar increase in metallicity.

As we only have $\sim$10 stars in that branch, we include the results of Nissen & Schuster (1997), who have studied 16 halo stars and 14 disk stars in the same metallicity range, with a precision comparable to ours. Their results for [Ca/Fe] versus [Fe/H] (excluding 4 stars with higher metallicity) are plotted together with ours in Fig. 8. The plots for other α-elements display similar behaviour. Figure 8 shows that there is indeed a small trend with [Fe/H] (-0.14), significantly smaller than the slope of ~ -0.5 which applies at higher metallicities. Should the same cause (enrichment by SNeI ejecta) explain the variation of [α/Fe] with [Fe/H] in both cases, one would expect

[1] It should be kept in mind, however, that the prediction of abundance ratios related to the heaviest elements remains fraught with uncertainties owing to the mass-cut issue.

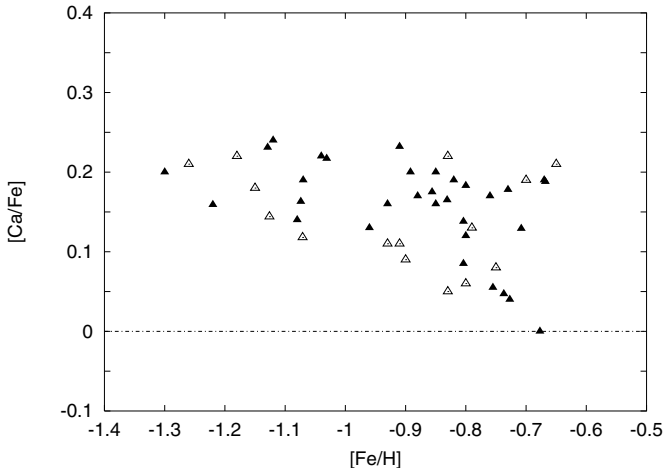

Fig. 8. [Ca/Fe] versus [Fe/H]. Results from this study and from Nissen & Schuster (1997) are plotted. Filled and open triangles represent disk and halo stars, respectively, the separation between the two populations having been set at a velocity of 150 km s^{-1} with respect to the Local Standard of Rest.

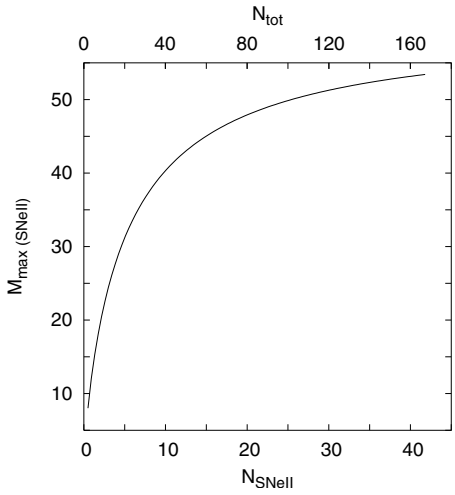

Fig. 9. Upper mass cutoff for a Salpeter IMF as a function of the total number of first generation stars in the cloud (upper abscissa) and of the total number of SNeII (lower abscissa). $M_{\rm max}$ is the mass above which the integrated IMF drops below 0.5, which means that the majority of the clouds will contain no star with mass > $M_{\rm max}$.

similar slopes, in contradiction with the observations. We thus conclude that the standard scenario cannot easily explain the observed variation of α/Fe along the Pop IIa branch.

3.5. Modified EASE scenario

Given the aforementioned drawbacks of both the original EASE scenario and the standard scenario, we propose a variant of the EASE scenario which is able to explain not only the observed α-elements ratios, but also the fact that only those stars displaying a maximum [α/Fe] can show *s*-process overabundances.

We assume that, in the protogalaxy, the primordial gas clouds (PGCCs) present a large mass range, with some clouds of mass much lower than the progenitors of the present day GCs. In the following, we examine what would happen, first in the massive, strongly bound clouds and, secondly, in the low mass, weakly bound clouds.

The massive clouds will probably be able to form a significant number of first generation stars, covering the whole mass range, from the lower limit (which could be 3 $M_\odot$ in zero metallicity gas, Nakamura & Umemura 1999) up to the highest masses. The stars with initial mass above 8 $M_\odot$ will explode as SNeII and trigger the formation of a second generation of stars in a supershell. Just as in the original EASE scenario, these second generation stars may or may not recollapse to form a bound globular cluster. As the SNeII cover the full mass range, from 8 $M_\odot$ up to the highest masses, the total production of α-elements can be obtained by integrating the yields over the full SNeII mass range, weighted by the IMF. Using the yields of Umeda & Nomoto (2002), we obtain maximum values of the ratios light/heavy α-elements (e.g., O/Si, Mg/Ca). These second generation stars will then lie at the right of the two-branches diagram (Pop IIb or maximum [α/Fe] Pop IIa stars).

On the other hand, the low-mass clouds will form only a small number of first generation stars. As a result, they might present a smaller fraction of very massive stars (e.g., $M >$ 30 $M_\odot$) than of lower mass ones (M between 8 and 30 $M_\odot$). One might assume that the IMF could change with the mass of the cloud, in such a way that the formation of very massive stars would be less likely in low mass clouds. However, such an assumption is not necessary. Indeed, even with a constant IMF, the expected number of very massive stars forming in clouds of decreasing mass will eventually drop below unity. If ones assumes a Salpeter IMF ranging from 3 to 60 $M_\odot$, Fig. 9 shows the upper mass cutoff as a function of the total number of stars and of the total number of SNeII. This upper mass cutoff is the mass above which the integrated IMF drops below 0.5, which means that the probability of forming a star above this mass is less than 50%. Thus, the majority of these clouds should not be able to form any star more massive than this cutoff.

For example, clouds with 20 first generation stars would, in general, contain 5 SNeII, but none of them would have an initial mass higher than 32 $M_\odot$. Such relatively small clouds would nevertheless be able to form a significant number of *second generation* stars, because of the high efficiency of star formation in a compressed gas of non-zero metallicity. However, these second generation stars would be formed from matter processed by SNeII of relatively low mass ($M < M_{\rm max}$), thus exhibiting lower values of light/heavy α-elements, as well as low values of [α/Fe].

These low mass clouds would have weak gravitational potentials. They would thus be unable to retain the AGB ejecta, and none of their stars would show signs of accreted material (*s*-process enhancements). This explains why only stars with maximum [α/Fe] can show *s*-process overabundances.

Moreover, these weakly bound clusters would be the most vulnerable to the Galactic tidal fields and, thus, the first disrupted (e.g., Gnedin & Ostriker 1997; Vesperini 1998). This explains why none of them seems to have survived until the present epoch. Since only the most massive and gravitationally bound GCs (thus having been enriched by very massive SNe)

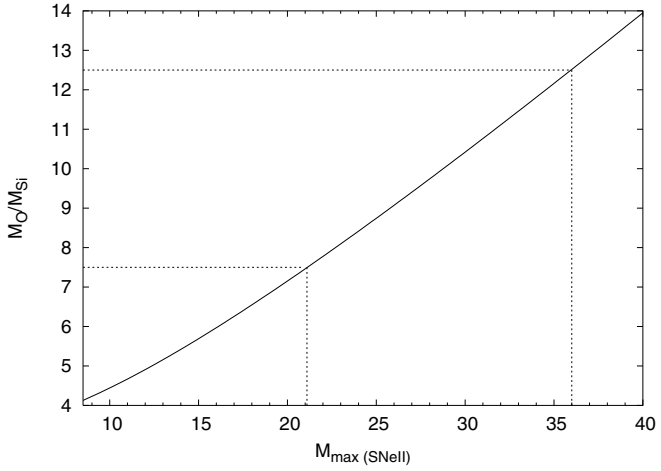

Fig. 10. Ratio of the yields of oxygen and silicon versus the upper mass cutoff for SNeII. These yields are integrated using the results of Umeda & Nomoto (2002), from 8 $M_\odot$ up to $M_{\max}$. The dotted lines correspond to the maximum range of M_O/M_{Si} obtained from our data, and thus correspond to an $M_{\max}$ varying between 21 and 36 $M_\odot$.

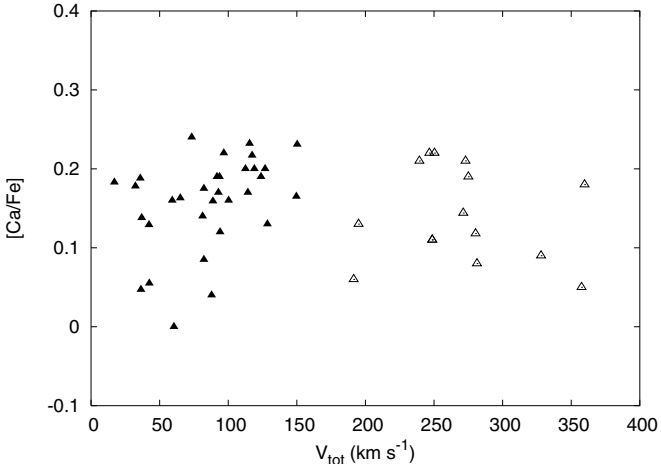

Fig. 11. [Ca/Fe] versus the modulus of the velocity with respect to the Local Standard of Rest (LSR). Results from this study and from Nissen & Schuster (1997) are plotted. Filled and open triangles represent disk and halo stars, respectively.

may have survived until the present time, this also explains why all present day GCs apparently display the same maximum value of α/Fe (see, for example, Thévenin et al. 2001).

Contrary to what was postulated in the original EASE scenario, the various [α/Fe] values along the Pop IIa branch would not correspond to a temporal sequence, but rather to stars originating from clusters with different initial masses, and thus a varying upper mass cutoff. As an example, on the basis of the yields calculated by Umeda & Nomoto (2002), we find that the lowest O/Si ratio we observe could be achieved with first generation stars whose mass does not exceed 21 $M_\odot$, while the highest ratio would require more massive stars (36 $M_\odot$ at least, see Fig. 10). These preliminary results confirm that a significant mass range for the PGCCs really could give rise to the observed ranges of [α/Fe] as well as of light/heavy α-elements.

Finally, let us come back to Fig. 8, which shows a small trend of [Ca/Fe] with metallicity. Indeed, Parmentier & Gilmore (2001), who studied the chemical enrichment of PGCCs with varying initial mass, predict that, the more massive the PGCCs, the lower the [Fe/H] achieved. Our modified EASE scenario, in which the most massive PGCCs would produce the highest [α/Fe] and the lowest [Fe/H], could therefore explain the small trend with metallicity which is observed in Fig. 8.

3.6. Abundance ratios versus kinematic properties

Another line of thought has been followed by several authors (e.g. Nissen & Schuster 1997; Bensby et al. 2003), who have argued that stars belonging to different populations (in kinematic terms) display different α/Fe. Bensby et al. (2003) show that thin disk stars display lower α/Fe than thick disk stars of the same metallicity. Nissen & Schuster (1997) find that, while thick disk stars display only high values of α/Fe, halo stars exhibit both high and low values at a given [Fe/H]. While the Bensby et al. (2003) analysis mostly concerns stars of metallicity higher than considered in the present study, the results of Nissen & Schuster (1997) are plotted together with ours in Fig. 11, which displays [Ca/Fe] as a function of the modulus of the velocity with respect to the Local Standard of Rest (LSR). It shows that some of the disk stars also exhibit low α/Fe, thus weakening the conclusion of Nissen & Schuster. On the basis of all the data discussed here, it does not seem that the kinematic properties play a significant role in α/Fe at metallicities below −0.6. However, this point deserves further investigation, and is the subject of an ongoing analysis.

3.7. Abundances in accreted matter

As mentioned in Sect. 1, according to the (revised) EASE scenario, the abundances in the atmospheres of Pop IIa stars should be representative of type II SN nucleosynthesis only, while the atmospheres of Pop IIb stars would also have been polluted by matter expelled by AGB stars. These two subpopulations are well separated by examination of the Y/Fe abundance ratio. The [C/Fe], [O/Fe] and [Na/Fe] abundances are plotted versus [Y/Fe] in Figs. 12–14.

While [Y/Fe] is expected to be an indicator of the amount of accreted matter in Pop IIb stars, it is not particularly relevant for Pop IIa. We thus examine the behaviour of Pop IIb only in Figs. 12–14 (the asterisks).

As for the other α-elements (see Jehin et al. 1999), [O/Fe] is constant in Pop IIb. This constancy suggests, as expected, that the oxygen abundance was not significantly modified by the nucleosynthetic processes which took place in the intermediate metal-poor AGB stars, that is, the stars assumed to be responsible for the pollution of our Pop IIb stars.

Now, considering the [C/Fe] and [Na/Fe] abundance ratios, we see an anticorrelation with [Y/Fe]. Indeed, the straight lines fitted through the Pop IIb data have slopes of about −0.5, and the correlation is significant at the 99% level. Thus, as [Y/Fe] increases, which means, according to our scenario, that the amount of accreted matter increases, [C/Fe] and [Na/Fe]

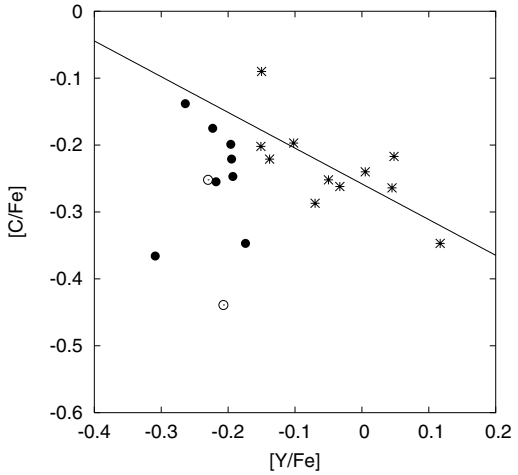

Fig. 12. Correlation diagrams for [C/Fe] versus [Y/Fe]. Symbols are the same as in Fig. 1. Also shown is the straight line fit through Pop IIb stars.

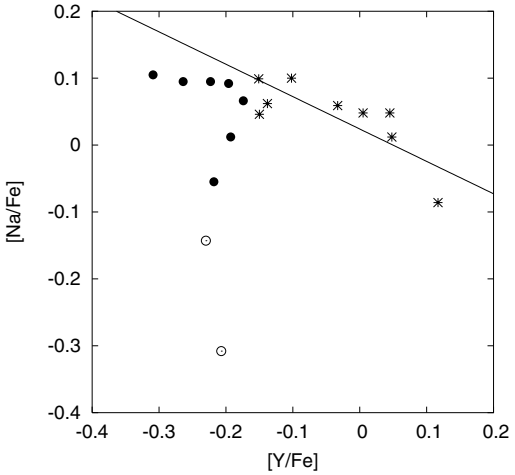

Fig. 14. Correlation diagrams for [Na/Fe] versus [Y/Fe]. Symbols are the same as in Fig. 1. Also shown is the straight line fit through Pop IIb stars.

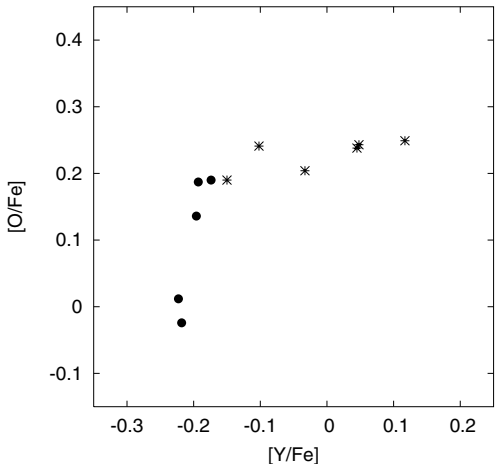

Fig. 13. Correlation diagrams for [O/Fe] versus [Y/Fe]. Symbols are the same as in Fig. 1.

decrease. We are thus led to postulate that the matter expelled by the AGB stars which populated the globular clusters in their early times was enriched in *s*-process elements, while carbon and sodium had been depleted by some nucleosynthetic process.

AGB stars produce their energy by alternatively burning hydrogen (CNO-cycle) and helium (3α reaction) in shells during the thermal pulses. The products of the helium burning shell (HeBS) are brought up to the star surface by the third dredge-up, leading to an enhancement of the surface carbon abundance. At the same time, *s*-elements are processed and also brought up to the star surface by the third dredge-up. On the other hand, when hydrogen is burnt by the CNO-cycle in the hydrogen burning shell (HBS), nitrogen is produced at the expense of carbon. If the still hypothetical process called "hot bottom burning" (HBB) takes place at this stage, the external convective envelope goes deep enough to be in contact with the HBS and some carbon is converted into nitrogen. When these products are brought up to the external layers, the surface abundance of carbon decreases. So, while *s*-element surface abundances are enhanced during this period, the carbon abundance is subject to two opposite processes: the third dregde-up which increases it, and the HBB which decreases it. According to Lattanzio et al. (2000), the HBB could occur in AGB stars more massive than 5 $M_{\odot}$. Moreover, it could also occur in less massive AGB stars of zero-metallicity (Siess et al. 2002). Our results thus suggest that, since we see an anticorrelation between the [C/Fe] and [Y/Fe] abundance ratios in the Pop IIb stars, the HBB really took place in most of the early globular cluster AGB stars.

Considering now the anticorrelation between the [Na/Fe] and [Y/Fe] abundance ratios, this is more difficult to explain in terms of the HBB. Indeed, along with the CNO-cycle in the HBS of AGB stars, the Ne-Na chain (as well as the Mg-Al chain) is expected to be active, leading to an enhancement of the Na abundance along with the carbon depletion. However, we see an *anti*-correlation Na-Y in the Pop IIb stars as well as an anticorrelation C-Y. Moreover, Al does not show any clear tendency with Y. Thus, it seems that, for still ill-determined reasons, the products of the chains usually accompanying the CNO-cycle were not brought up to the AGB star surface.

4. Concluding remarks

Our new abundance results, added to those of Jehin et al. (1999), have made it possible to shed more light on the formation of mildly metal-poor stars.

First, a detailed examination of the correlations between the α-element abundances has prompted us to propose a modification of the EASE scenario, in which the different α/Fe ratios are no longer explained by the different times at which the stars form in the proto-globular clouds, but rather by the large mass range of the progenitor clouds.

On the other hand, the anticorrelation between carbon and the *s*-elements suggests that the so-called "hot-bottom burning" may play an important role in massive low-metallicity AGB stars.

Obviously, more investigations, both the theoretical and observational, are needed to better understand the detailed abundances of intermediate metallicity stars, which, in our opinion, constitute a very good laboratory for testing the Galactic chemical evolution models.

Acknowledgements. H.D. is financially supported by FRIA (Brussels, Belgium). This work has also been supported by contract Pôle d'Attraction Interuniversitaire P5/36 (PPS Science Policy, Belgium).

References

Bensby, T., Feltzing, S., & Lundström, I. 2003, A&A, 410, 527
Brown, J. H., Burkert, A., & Truran, J. W. 1995, ApJ, 440, 666
Cavallo, R. M., Pilachowski, C. A., & Rebolo, R. 1997, PASP, 109, 226
Delbouille, L., Roland, G., & Neven, L. 1973, Photometric Atlas of the Solar Spectrum from 3000 Å to 10 000 Å, Institut d'Astrophysique, Université de Liège, Belgium
Gnedin, O. Y., & Ostriker, J. P., ApJ, 474, 223
Goriely, S., & Siess, L. 2001, A&A, 378, L25
Gratton, R. G., Carretta, E., Claudi, R., Lucatello, S., & Barbieri, M. 2003, A&A, 404, 187
Iwamoto, K., Brachwitz, F., Nomoto, K., et al. 1999, ApJS, 125, 439
Jehin, E., Magain, P., Neuforge, C., et al. 1999, A&A, 341, 241
Larson, R. B. 1998, MNRAS, 301, 569
Lattanzio, J., Forestini, M., & Charbonnel, C. 2000, Mem. Soc. Astron. It., 71, 737
Nakamura, F., & Umemura, M. 1999, ApJ, 515, 239
Nissen, P. E., & Schuster, W. J. 1997, A&A, 326, 751
Nissen, P. E. 1999, Ap&SS, 265, 249
Nissen, P. E., Primas, F., Asplund, M., & Lambert, D. L. 2002, A&A, 390, 235
Parmentier, G., Jehin, E., Magain, P., et al. 1999, A&A, 352, 138
Parmentier, G., Jehin, E., Magain, P., Noels, A., & Thoul, A. A. 2000, A&A, 363, 526
Parmentier, G., & Gilmore, G. 2001, A&A, 378, 97
Parmentier, G. 2004, MNRAS, 351, 585
Siess, L., Livio, M., & Lattanzio, J. 2002, ApJ, 570, 329
Thévenin, F., Charbonnel, C., de Freitas Pacheco, J. A., et al. 2001, A&A, 373, 905
Umeda, H., & Nomoto, K. 2002, ApJ, 565, 385
Vesperini, E. 1998, MNRAS, 299, 1019